Acta Geochim (2017) 36(2):151–165
DOI 10.1007/s11631-017-0141-y

ORIGINAL ARTICLE

Ore-forming elements diffusion and distribution in the altered host rock surrounding the Koktokay No. 3 pegmatite in the Chinese Altay

Jingyu Zhao[1,2] · Hui Zhang[1] · Yong Tang[1] · Zhenghang Lü[1] · Yang Chen[3]

Received: 28 October 2016 / Revised: 23 December 2016 / Accepted: 16 January 2017 / Published online: 14 February 2017

Abstract Petrography and geochemistry of the altered and unaltered host rocks surrounding the Koktokay No. 3 pegmatite revealed that the unaltered amphibolite is mainly composed of hornblende, plagioclase, and ilmenite. Beyond these primary components, the altered host rocks contain a few newly formed minerals, including biotite, tourmaline, chlorine, and muscovite. The alteration zone surrounding the Koktokay No. 3 pegmatite is limited to 2.0 m, characterized by biotitization, tourmalization, and chloritization. In the altered host rocks, the contents of SiO_2, MgO, MnO, Na_2O, and TiO_2 did not vary greatly. However, Al_2O_3 showed a weak decreasing trend with the increasing distance from the pegmatite contact zone, while Fe_2O_3 and CaO showed an increasing trend. The contents of Li, Rb, and Cs in the altered host rocks were much higher than those in the unaltered host rocks, decreasing with distance from the contact. The chondrite-normalized rare earth element (REE) pattern of the altered and unaltered host rock was right-inclined from La to Lu, but enriched in light REEs over heavy REEs after hydrothermal alteration. An isocon plot shows that some oxides migrated in with an order of $P_2O_5 > K_2O > TiO_2 > Al_2O_3 > SiO_2 > MnO \geq MgO$, while others migrated out with an order of $Na_2O > CaO > Fe_2O_3$. For REEs, the migration ratios are positive values with Cs > Rb > Li > Nb > Ta > Be, signifying that all REEs migrated from the exsolved magmatic fluid into the altered host rocks. It was concluded that diffusion was the only mechanism for migration of ore-forming elements in the alteration zone. The effective diffusion coefficients (D_{eff}) of LiF, RbF, and CsF were estimated under a fluid temperature of 500–550 °C. Using a function of concentration ($C_{(x,t)}$) and distance (x), the order of migration distance was determined to be LiF > CsF > RbF, with diffusion times of $(3.39 \pm 0.35) \times 10^6$, $(3.19 \pm 0.28) \times 10^5$ and $(6.33 \pm 0.05) \times 10^5$ years, respectively.

Keywords Rare elements · Diffusion · Alteration · Koktokay No. 3 pegmatite · Altay

1 Introduction

When a rare-element pegmatite intrudes country rock (e.g., mafic metavolcanic rocks or metasedimentary rocks), rare-element-enriched fluid interacts with the country rock to form a metasomatic or dispersion halo (Selway and Breaks 2005). As the host rock is characterized by enrichment of highly mobile alkali elements (i.e., Li, Rb, Cs) and volatile components (i.e., H_2O, B, F), bulk whole-rock analysis of metasomatically altered host rocks is an effective exploration tool for finding hidden or blind pegmatites (Cerný 1989; Selway and Breaks 2005). Li is the most mobile element in most rare-element-mineralized systems, and altered halos formed by Li diffusion in different host rocks many times larger than the pegmatite bodies themselves have been reported in the Superior Province of Ontario, Canada (Breaks and Tindle 1997).

Metasomatized host rocks adjacent to a rare-element pegmatite (or exocontact) commonly have abnormal

✉ Hui Zhang
zhanghui@vip.gyig.ac.cn

1 Key Laboratory of High-Temperature and High-Pressure Study of the Earth's Interior, Institute of Geochemistry, Chinese Academy of Sciences, Guiyang 550081, China

2 University of Chinese Academy of Sciences, Beijing 100049, China

3 Zhejiang University, Hangzhou 310058, China

altered mineral assemblages, including holmquistite, (Li, Rb, Cs)-rich biotite, and/or tourmaline (Selway and Breaks 2005; Chen et al. 2016). These minerals occur in altered mafic metavolcanic host rocks due to the influx of rare-element fluids (London et al. 1996), with holmquistite being an excellent exploration indicator because it only occurs in metasomatized host rocks within 10 m of a rare-element pegmatite (London 1986). Breaks et al. (2003) proposed that a K/Rb versus Cs plot is useful for evaluating the degree of metasomatism of the host rock, for metasomatic biotite associated with rare-element pegmatites is characterized by enrichment of Rb and Cs, yielding values of K/Rb < 10 and Cs > 1000 ppm.

There are more than 100,000 pegmatite veins distributed in the Chinese Altay, including the Koktokay No. 3 which is the largest and most highly evolved LCT-type pegmatite in the world (Zou et al. 1986; Liu and Zhang 2005), hosting a super-large Li–Be–Nb–Ta–Cs–Rb–Hf deposit (Zou and Li 2006). The intrusion age and magmatic-hydrothermal evolution of the pegmatite have been clarified through recent geochemical studies (Lu et al. 1996; Zhu et al. 2000, 2006; Zhang 2001; Zhang et al. 2004; Wang et al. 2007, 2009; Chen 2011; Liu et al. 2014; Che et al. 2015; Wu et al. 2015). Previous studies have shown that the Koktokay No. 3 pegmatite formed in the Triassic (220–212 Ma) and that the pegmatite-forming initial magma contains 2.5 wt%–3.2 wt% B_2O_3, 5.4 wt%–6.8 wt% P_2O_5, and 0.3%–0.4% F. Koktokay No. 3 has been divided into magmatic (zone I–IV), magmatic–hydrothermal transition (zone V–VIII), and hydrothermal (zone IX) stages.

There has been little research on the distribution of rare-metal elements with increasing distance from the contact between pegmatite and host rock, and the implications thereof for exploration of rare-metal ore deposits in the Chinese Altay. Recently, a rare elements diffusion model in the altered host rock of biotite-quartz schist (Kulumuti group, S_{2-3}KL) was established, based on the intrusion of No. 807 pegmatite in the Kaluan ore field (Chen et al. 2016). However, the amphibolite host rock of the Koktokay No. 3 pegmatite was formed by metamorphism of gabbro, differentiating it from the metasedimentary rocks exposed in the Kaluan pegmatite field. It is therefore necessary to set up a new diffusion model and determine the distribution of rare elements in metasomatic alteration based on petrological, mineralogical, and geochemical studies of the host rock.

2 Geological background

2.1 Regional geology

The Chinese Altay orogenic belt consists of Ordovician to Devonian clastic sedimentary and volcanic rocks and their metamorphic equivalents, extending eastward to Mongolia and westward to Kazakhstan and Russia (Windley et al. 2002, 2007; Xiao et al. 2004; Long et al. 2007, 2008, 2010; Sun et al. 2008, 2009). The Chinese Altay was in a stable continental margin from the Late Precambrian to the Early Paleozoic before its orogenic movement started in the Early Paleozoic. The orogenic movement lasted into the Late Paleozoic, with subduction, collision, and accretion in succession. On the basis of stratigraphy, metamorphism, deformation pattern, magmatic activity, and geochronology, the Chinese Altay can be divided into five fault-bounded terranes (Terranes 1–5, Fig. 1), separated by the Hongshanzui, Kalaxianger, Abagong-Kurit, and Maerkakuli Faults, respectively. Terrane 1 is made up of Late Devonian to Early Carboniferous clastic sediments, limestones, and some minor island-arc volcanic rocks metamorphosed to the lower greenschist facies; Terrane 2 is composed of a Middle Ordovician turbidite sequence also of the lower greenschist facies; Terrane 3 is the largest terrane and is comprised of Early Paleozoic sediments metamorphosed at medium-to-high grade; Terrane 4 consists of Devonian turbiditic sandstone, pillow basalts, and some siliceous volcanic rocks; and Terrane 5 is mainly composed of Devonian fossiliferous successions that are, in turn, overlain by Late Carboniferous formations (Sengör et al. 1993; Long et al. 2007; Yuan et al. 2007; Sun et al. 2008; Cai et al. 2011a, b).

About 200 granitoid plutons varying from metaluminous granodioritic to weakly peraluminous, mica-rich granitic (Cai et al. 2011b) occupy more than 40% of the Chinese Altay (Zou et al. 1989), indicating that strong magmatism occurred in the development of the Chinese Altay (Zou et al. 1989; Wang et al. 1998).

More than 100,000 pegmatite veins occur in the Chinese Altay and some of them host large or super-large rare metal deposits (Zou et al. 1989; Zou and Li 2006). The pegmatites are divided into 38 pegmatite fields, of which the Koktokay pegmatite field is the most important.

2.2 Geology of the mining area

The Koktokay mining area (Fig. 2) is located at the bulge of the Southwestern Koktokay pegmatite field. In the −7-km^2 area, there are 25 pegmatite veins; 11 of them host rare metal deposits and are characterized by rare-metal pegmatites intruded into the metagabbro. The exposed strata in the mining area is Habahe group ($O_{2-3}hb$), mainly composed of staurolite-bearing biotite–plagioclase–quartz schist, andalusite–bearing biotite–quartz schist, and quartz–biotite schist. Basic rocks are mainly clustered in the midwest of the mining area with an intrusion age of 408 ± 6 Ma (Wang et al. 2006), with amphibolite in the east and metagabbro in the west. In addition, gneissic

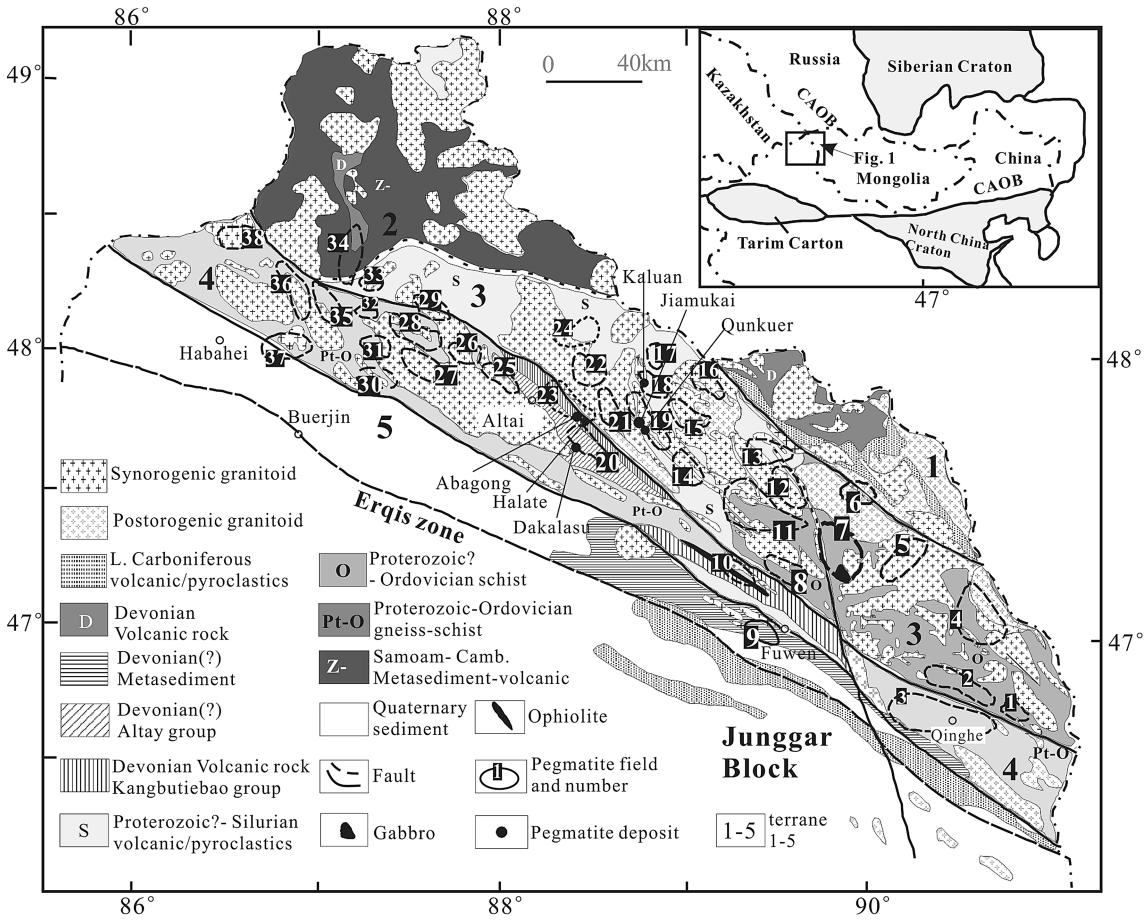

Fig. 1 Geological sketch map of the Chinese Altay orogen (modified from Wang et al. 2006; Zou and Li 2006)

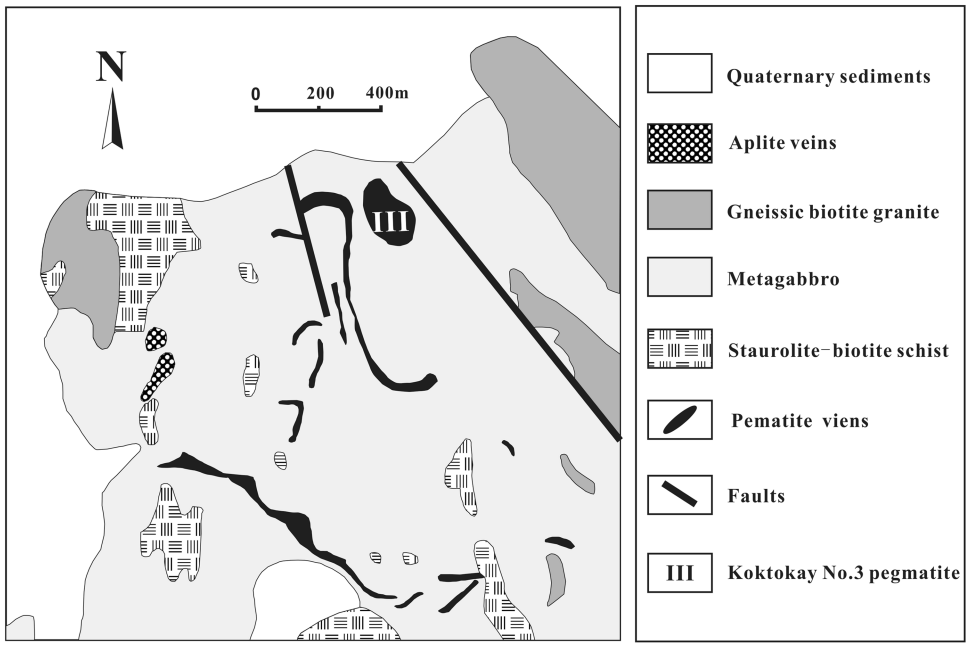

Fig. 2 Geological sketch map of the Koktokay No. 3 pegmatite (modified from Zhu et al. 2000)

granite with an intrusion age of 399 ± 2 Ma is distributed extensively throughout the mining area (Wang et al. 2006; Cai et al. 2011b).

The Koktokay No. 3 pegmatite, located at the junction between the NW-trending Erqis Fault and NNW-trending Kalaxianger Fault, is composed of a gently dipping "plate" and a steeply dipping "cupola" protruding from the plate upwards. The cupola-shaped part is 250 m × 250 m × 250 m depth, with a strike of NW 335°, NE inclination, and dip angle of 75°–90°, and showing a typical concentric ring structure of nine textural zones from the rim to its core. Based on the occurrence of Li-dominant minerals (e.g., spodumene, lepidolite, and elbaite), zones I to IV were named as the outer pegmatite and zones V to IX were named as the inner pegmatite. A several-centimeter-wide contact zone occurs between the pegmatite and the surrounding amphibolite. Adjacent to the contact zone, the amphibolite contains an alteration halo of Li, Rb, Cs, F, and B.

3 Sampling and analytical methods

3.1 Sample collection

The Koktokay No. 3 pegmatite had been mined for beryl, spodumene, lepidolite, and columbite-tantalite by a Chinese-Soviet mining company since 1950 (Zhu et al. 2000), but activity ceased at the end of 1999 due resource exhaustion of the cupola part of the pegmatite and the open pit filled with water. The site was re-opened for beryl mining in the plate part of the pegmatite in 2011. As the specimen repository collapsed in heavy snow in the 1980s, drill core samples were not available for this study.

The contact between the Altay pegmatites and their host rocks is sharp, with narrow metasomatic halos (alteration zones) developed in the host rocks. A well-preserved profile was selected for sample collection from the wall on the west side of the open pit at 1186 m, including the pegmatite itself, border zone, internal- and external-contact zones, and altered host rocks. The freshest samples possible were collected. In addition, care was taken to avoid samples from the selected profile that may have been affected by other pegmatite dikes. Five altered host rocks were picked at 0.0 m (the external contact zone), 0.5, 1.0, 1.5, and 2.0 m from the contact between the pegmatite and host rock and numbered Kp03-alt-01, -02, -03, -04, and -05, respectively. Three host rock samples represent the unaltered amphibolite. These were numbered Kp03-hr-01, -02 and -03, respectively, and collected far from the pegmatite contact (> 50 m), with Kp03-hr-02 on the transect of altered samples.

3.2 Analytical methods

All samples (including five altered and three unaltered host rocks) were analyzed for main chemical composition and trace element content at the State Key Laboratory of Ore Deposit Geochemistry, Institute of Geochemistry, Chinese Academy of Sciences, Guiyang. The main chemical compositions were analyzed by X-ray fluorescence spectrometry (XRF) after powder samples were prepared by the fusion method. Trace elements were measured by inductively coupled plasma mass spectrometer (ICP–MS) after sample digestion using a mixture of HF and HNO_3 acids in high-pressure "bombs" (Liang et al. 2000). Rh standard solutions were added as the internal calibration to monitor instrument drift. Several reference materials (G2, G3, GSD-12, GSR-1, GSR-2, GSR-3, SY4, W-2, and SARM-4) were measured together with unknown samples. The relative standard deviation (RSD) of XRF and ICP-MS analyses were less than ±2% and ±5%, respectively, for main chemical composition and trace elements in this study.

Polished thin sections were prepared for observation. Petrographic textures were observed using back-scattered electron (BSE) mode with a JEOL 8100 electron probe micro-analyzer (EPMA) at Chang'an University. Mineral compositions were measured using the EPMA in wavelength-dispersion spectroscopic (WDS) mode. The microprobe was operated at an accelerating voltage of 15 kV and a beam current of 10 nA. Peak and background counting times for most elements were 10 and 5 s, respectively. All data were reduced using the ZAF program. The RSD of the EMPA analyses was less than ±2%.

4 Results

4.1 Petrography of the altered and unaltered host rocks

Micrographs of the altered and unaltered host rocks are shown in Fig. 3; relative mineral contents (vol%), EMPA chemical compositions (wt%) of the rock-forming and accessory minerals, and calculated chemical compositions of altered and unaltered host rocks are listed in Table 1.

According to the petrographic observations of the three unaltered host rocks, unaltered amphibolite is mainly composed of hornblende (50 vol%–55 vol%), plagioclase (40 vol%–45 vol%), ilmenite (3 vol%), and a small amount of quartz and chlorite (Table 1; Fig. 3a). With the exceptions of hornblende, plagioclase, and ilmenite, we observed few newly formed minerals, such as biotite, tourmaline, chlorine, and/or muscovite, representing minerals produced in the hydrothermal alteration (Fig. 3b–f). In this study, alteration types of biotitization, tourmalization and chloritization, are

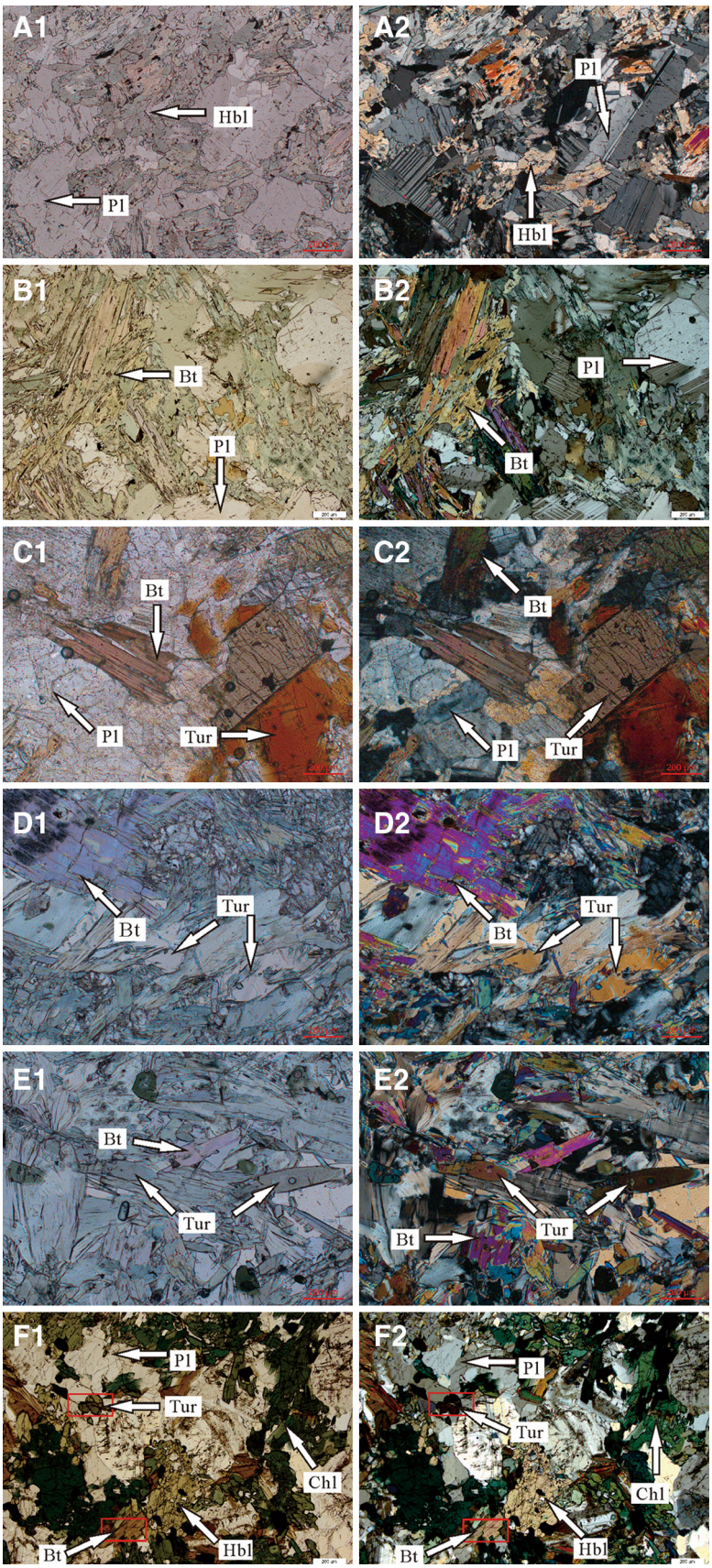

Fig. 3 Photomicrograph of sample. Notes: **a** Kp03-hr-02; **b** Kp03-alt-01; **c** Kp03-alt-02; **d** Kp03-alt-03; **e** Kp03-alt-04; **f** Kp03-alt-05; *1* plane-polarized light; *2* cross-polarized light

Table 1 Statistical results of the relative mineral contents (vol%), EMPA results of chemical compositions (wt%) of the rock-forming and accessory minerals, and calculated chemical compositions of altered and unaltered host rocks surrounding the Koktokay No. 3 pegmatite

Sample no.	Kp03-alt-01					Kp03-alt-02							Kp03-alt-03					
Mineral Content (vol%)	Hbl 36	Pl 34	Bio 22	Chl 5	Ilm 3	Hbl 41	Pl 32	Bio 8	Tour 10	Mus 3	Chl 3	Ilm 3	Hbl 47	Pl 31	Bio 10	Tour 8	Chl 1	Ilm 3
SiO_2	46.81	54.81	39.37	29.52	/	47.52	57.87	38.72	35.85	48.03	27.77	/	45.66	58.59	38.09	36.22	27.54	0.06
TiO_2	0.29	0.53	0.87	0.05	48.50	0.55	0.01	0.77	0.75	/	0.03	48.69	0.50	/	1.47	0.78	0.04	47.63
Al_2O_3	11.23	29.23	17.65	20.64	0.02	10.70	26.28	17.55	30.25	37.59	22.89	0.01	11.77	26.27	18.58	29.82	22.81	0.00
FeO	13.97	0.08	13.09	13.26	49.28	15.62	0.05	17.70	7.67	0.52	13.08	47.90	12.64	0.00	15.67	7.58	13.19	46.27
MnO	0.19	/	0.10	0.16	1.77	0.31	/	0.07	0.05	0.03	0.12	1.57	0.16	/	0.08	0.04	0.13	4.83
MgO	11.59	/	15.57	21.70	0.23	11.26	0.02	12.25	7.51	0.46	22.42	0.11	12.30	/	13.06	7.72	22.01	0.13
CaO	11.04	10.65	0.02	0.10	/	11.87	8.74	0.03	1.93	0.08	0.02	0.00	12.46	8.45	0.06	2.35	0.04	/
Na_2O	1.39	4.99	0.44	0.12	0.02	1.19	7.64	0.23	2.36	0.09	0.05	0.04	1.98	7.70	0.18	1.42	0.07	0.01
K_2O	0.20	0.06	6.48	0.20	/	0.23	0.07	7.38	/	8.16	0.03	/	0.33	0.07	7.72	0.04	0.05	/
P_2O_5	0.04	0.02	0.04	0.02	/	0.02	0.03	0.05	/	0.07	0.03	/	0.08	/	0.03	/	0.02	/
Total	96.74	100.37	93.63	85.77	99.82	99.25	100.70	94.74	86.35	95.03	86.45	98.32	97.87	101.08	94.95	85.97	85.90	98.93
Chemical compositions of the altered host rocks based on mineral chemical calculation																		
SiO_2	45.62					46.95							46.60					
TiO_2	1.93					1.83							1.87					
Al_2O_3	18.90					19.04							18.15					
FeO	10.08					10.44							9.63					
MgO	8.69					7.04							7.93					
CaO	7.60					7.86							8.67					
K_2O	1.53					0.95							0.95					

Sample no.	Kp03-alt-04						Kp03-alt-05							Kp03-hr-02				
Mineral Content (vol%)	Hbl 44	Pl 34	Bio 9	Tour 9	Chl 1	Ilm 3	Hbl 45	Pl 34	Bio 4	Tour 3	Chl 9	Ilm 3	Qz 2	Hbl 51	Pl 43	Chl 1	Ilm 3	Qz <1
SiO_2	49.87	48.60	37.81	36.06	27.69	/	50.20	53.94	38.32	35.85	26.77	0.06	97.83	55.39	46.67	27.82	/	100.40
TiO_2	0.38	0.03	1.86	0.86	0.04	54.04	0.37	/	2.02	1.05	0.10	50.07	/	/	/	0.07	48.50	/
Al_2O_3	8.52	32.13	17.16	30.13	22.55	0.01	8.51	29.39	17.55	30.03	22.37	0.04	0.02	2.63	34.97	23.13	0.02	0.01
FeO	16.95	0.09	17.04	7.58	13.15	44.92	16.98	0.08	17.60	7.67	16.41	48.76	0.04	18.56	0.07	15.81	49.28	0.07
MnO	0.55	0.04	0.13	0.03	0.07	1.89	0.50	/	0.09	0.05	0.22	2.40	/	0.73	0.00	0.11	1.77	/
MgO	14.55	0.03	12.24	7.50	23.09	0.02	13.86	/	11.75	7.51	19.88	0.10	0.02	17.49	/	19.40	0.23	0.01
CaO	5.73	15.75	0.05	2.45	0.01	0.06	7.00	11.85	0.09	2.36	0.08	0.03	0.06	1.41	17.63	0.01	/	0.05
Na_2O	0.93	2.98	0.21	1.47	0.07	0.04	0.87	5.91	0.21	1.34	0.06	0.07	0.10	0.05	1.42	0.04	0.02	0.01
K_2O	0.10	0.05	8.20	0.02	0.06	0.01	0.19	0.06	8.38	0.01	0.04	/	0.07	0.02	0.01	0.01	/	0.01
P_2O_5	0.04	0.04	0.06	/	0.03	/	0.02	0.02	0.07	/	0.03	/	0.04	/	0.02	0.01	/	0.02

Table 1 continued

Sample no.	Kp03-alt-04						Kp03-alt-05							Kp03-hr-02					
Mineral	Hbl	Pl	Bio	Tour	Chl	Ilm	Hbl	Pl	Bio	Tour	Chl	Ilm	Qz	Hbl	Pl	Chl	Ilm	Qz
Content (vol%)	44	34	9	9	1	3	45	34	4	3	9	3	2	51	43	1	3	<1
Total	97.61	99.73	94.77	86.10	86.75	100.99	98.49	101.25	96.08	85.85	85.96	101.54	98.17	96.27	100.80	86.42	99.82	100.57
Chemical compositions of the altered and unaltered host rocks based on mineral chemical calculation																		
SiO_2	45.39						47.90							48.59				
TiO_2	2.04						1.79							1.46				
Al_2O_3	19.15						17.44							16.61				
FeO	11.18						11.54							11.14				
MgO	8.42						8.72							9.12				
CaO	8.10						7.26							8.30				
K_2O	0.80						0.44							0.01				

/ below detection, *Hbl* hornblende, *Pl* plagioclase, *Bio* biotite, *Mus* muscovite, *Tour* tourmaline, *Ilm* ilmenite, *Chl* chlorite, *Qtz* quartz

defined based on the relative contents of the newly formed minerals (biotite, tourmaline, chlorite >5 vol%). The external contact zone sample (Kp03-alt-01) was characterized by abnormally high biotite content (22 vol%) (Fig. 3b), and the altered host rock at 2.0 m away from the contact (Kp03-alt-05) had abnormally high chlorite content (9 vol%) (Fig. 3f). Other altered host rocks (including Kp03-alt-02, -alt-03, and -alt-04) returned higher mineral content of tourmaline (8 vol%–10 vol%) and biotite (8 vol%–10 vol%) (Table 1; Fig. 3c–e). Tourmalines, characterized by complex and variable pleochroic zoning, formed fine- to medium-grained prisms in altered host rocks, associated with fine-grained biotite at some locations. The chemical compositions of tourmalines in the altered host rocks classified them as dravite. Biotite and muscovite were both found in a strongly altered host rock (Kp03-alt-02), in which muscovite (3 vol%) was contoured, and fine in size; and biotite, showing colorless to pale gray–brown pleochroism, was pervasive, and fine-grained in size.

The chemical compositions of hornblende from the altered host rocks were different from the unaltered host rocks, characterized by abnormally high contents of Al_2O_3 (8.51 wt%–11.77 wt%), CaO (5.73 wt%–11.04 wt%), Na_2O (0.87 wt%–1.39 wt%), and K_2O (0.10 wt%–0.33 wt%), and low contents of SiO_2 (45.66 wt%–50.20 wt%), FeO (12.64 wt%–16.98 wt%), and MgO (11.26 wt%–14.55 wt%) (Table 1). Moreover, plagioclase compositions had less Al_2O_3 (26.27 wt%–32.13 wt%) and CaO (8.45 wt%–15.75 wt%), and more SiO_2 (48.60 wt%–58.59 wt%) and Na_2O (2.98 wt%–7.70 wt%) in the altered host rocks as compared with unaltered host rock (46.67 wt% SiO_2, 34.97 wt% Al_2O_3, 17.63 wt% CaO, and 1.42 wt% Na_2O) (Table 1). The chemical compositional variations of hornblende and plagioclase in the altered host rocks indicate that dissolution and recrystallization of these two minerals were involved during the process of hydrothermal alteration.

4.2 Geochemical features of the altered host rocks

The main chemical compositions of the altered and unaltered host rocks are listed in Table 2. The unaltered host rocks contained low contents of SiO_2 (44.85 wt%–46.01 wt%), Na_2O (1.76 wt%–2.02 wt%), and K_2O (0.36 wt%–0.42 wt%) and high contents of Al_2O_3 (15.79 wt%–16.35 wt%), Fe_2O_3 (14.89 wt%–16.05 wt%), MgO (7.33 wt%–7.99 wt%), and CaO (8.39 wt%–9.49 wt%). Compared with the unaltered host rocks, the altered host rocks had more SiO_2 (46.94 wt%–49.86 wt%), TiO_2 (1.73 wt%–1.97 wt%), Al_2O_3 (16.39 wt%–18.30 wt%), K_2O (0.39 wt%–2.12 wt%), P_2O_5 (0.15 wt%–0.80 wt%), and less Fe_2O_3 (12.43 wt%–15.62 wt%), MgO (6.23 wt%–7.67 wt%), CaO (6.75 wt%–7.72 wt%), and Na_2O (0.75 wt%–1.15 wt%). In the altered host rocks,

Table 2 Main chemical compositions (in wt%) of altered and unaltered host rocks surrounding the Koktokay No. 3 pegmatite

Sample no.	Kp03-alt-01	Kp03-alt-02	Kp03-alt-03	Kp03-alt-04	Kp03-alt-05	Kp03-hr-01	Kp03-hr-02	Kp03-hr-03
SiO_2	47.55	48.53	49.86	47.55	46.94	44.85	46.01	44.95
TiO_2	1.93	1.93	1.73	1.97	1.83	1.34	1.63	1.34
Al_2O_3	18.15	18.30	17.65	18.05	16.39	16.28	15.79	16.35
Fe_2O_3	12.43	13.28	13.01	13.65	15.62	16.05	14.89	15.71
MgO	6.73	6.54	6.23	6.75	7.67	7.41	7.99	7.33
CaO	6.75	7.17	7.52	7.72	7.35	9.49	8.39	9.24
Na_2O	1.09	1.02	0.97	1.15	0.75	2.02	1.76	1.92
K2O	2.12	0.72	0.85	0.77	0.39	0.42	0.36	0.39
MnO	0.17	0.19	0.15	0.15	0.20	0.18	0.18	0.18
P_2O_5	0.65	0.27	0.64	0.80	0.15	0.06	0.18	0.06
L.O.I	2.81	2.59	2.59	2.53	2.38	1.85	2.71	2.47
Total	100.43	100.03	100.48	99.97	100.64	99.97	100.50	100.15

L.O.I loss on ignition

with x (distance away from the pegmatite contact) increasing from 0.0 to 2.0 m, SiO_2, MgO, MnO, Na_2O, and TiO_2 contents did not vary significantly (Fig. 4). As x increased from 0.0 to 2.0 m, Al_2O_3 showed a weak decreasing trend from 18.15 wt% to 16.39 wt% (Fig. 4b), whereas Fe_2O_3 and CaO showed increasing trends from 12.43 wt% to 15.62 wt% (Fig. 4c) and from 6.75 wt% to 7.35 wt% (Fig. 4e), respectively.

The maximum and minimum values of K_2O (2.24 wt% and 0.39 wt%) were observed at $x = 0.0$ m and $x = 2.0$ m (Fig. 4g), corresponding to the strongest biotitization and chloritization in host rocks; however, K_2O in the altered host rocks at $x = 0.5$–1.5 m showed constant values within error, consistent with a similar mineral content of mica in samples (8% Bio + 3% Mus in Kp03-alt-02, 10% Bio in Kp03-alt-03, and 9% Bio in Kp03-alt-04).

4.3 Distribution of REE and rare elements in the altered host rocks

REE (including Y) and rare element contents of the altered and unaltered host rocks are listed in Table 3. Li, Rb, and Cs contents in the altered host rocks were much higher than those in the unaltered host rocks, and all had a decreasing trend as x increased. The maximum values were at $x = 0.0$ m, with 693 ppm Li, 160 ppm Rb and 81.8 ppm Cs (Fig. 5a–c). Similarly, Be, Nb, and Ta decreased with tre increasing x, with maximum values at $x = 0.0$ m: 2.87 ppm Be, 11.2 ppm Nb, and 0.68 ppm Ta.

REE (including Y) content in the unaltered host rock was 70.08 ppm, with small negative Eu anomalies ($\delta Eu = 0.93$). The altered host rocks at $x = 0.0$, 1.0, and 1.5 m had high REE (Y), in the range of 88.82–104.33 ppm, with very weak Eu anomalies ($\delta Eu = 0.87$–1.12); whereas the other two altered host rocks at $x = 0.5$ and 2.0 m had lower contents of REE (Y), ranging from 50.62 to 51.82 ppm, with strong positive Eu anomalies ($\delta Eu = 1.42$–1.84). The chondrite-normalized REE content of the unaltered host rock shows a right-inclined pattern from La to Lu, characterized by $(La/Sm)_N$, $(La/Gd)_N$, and $(La/Yb)_N$ values of 1.75, 2.25, and 2.92, respectively. The weakly altered host rock at $x = 2.0$ m (Kp03-alt-05) show a similar REE pattern as the unaltered host rock with $(La/Sm)_N$, $(La/Gd)_N$, and $(La/Yb)_N$ values of 1.92, 2.29, and 2.86, respectively. Other altered host rocks at $x = 0.0$–1.5 m have similar chondrite-normalized REE patterns (Fig. 6), with larger $(La/Sm)_N$, $(La/Gd)_N$, and $(La/Yb)_N$ values (2.19–3.07, 2.72–3.88, and 6.20–9.64, respectively) than those in the unaltered host rock (Table 3).

Except for the weakly altered host rock, large $(La/Yb)_N$ values in altered host rocks ($x = 0.0$–1.5 m) indicate enrichment of light REEs over heavy REEs during hydrothermal alteration.

5 Discussion

5.1 The associated alteration reaction

The hydrothermal alteration zone of the host rocks, which originated from the intrusion and evolution of the Koktokay No. 3 pegmatite, is only in the range of 2.0 m, characterized by biotitization and tourmalization. Chloritization was the product of low temperature hydrothermal alteration. Compared with the mineral composition of the unaltered host rock, the decreasing mineral contents of hornblende and plagioclase and occurrence of newly formed minerals in the altered host rocks indicate dissolution of hornblende and plagioclase, and formation of

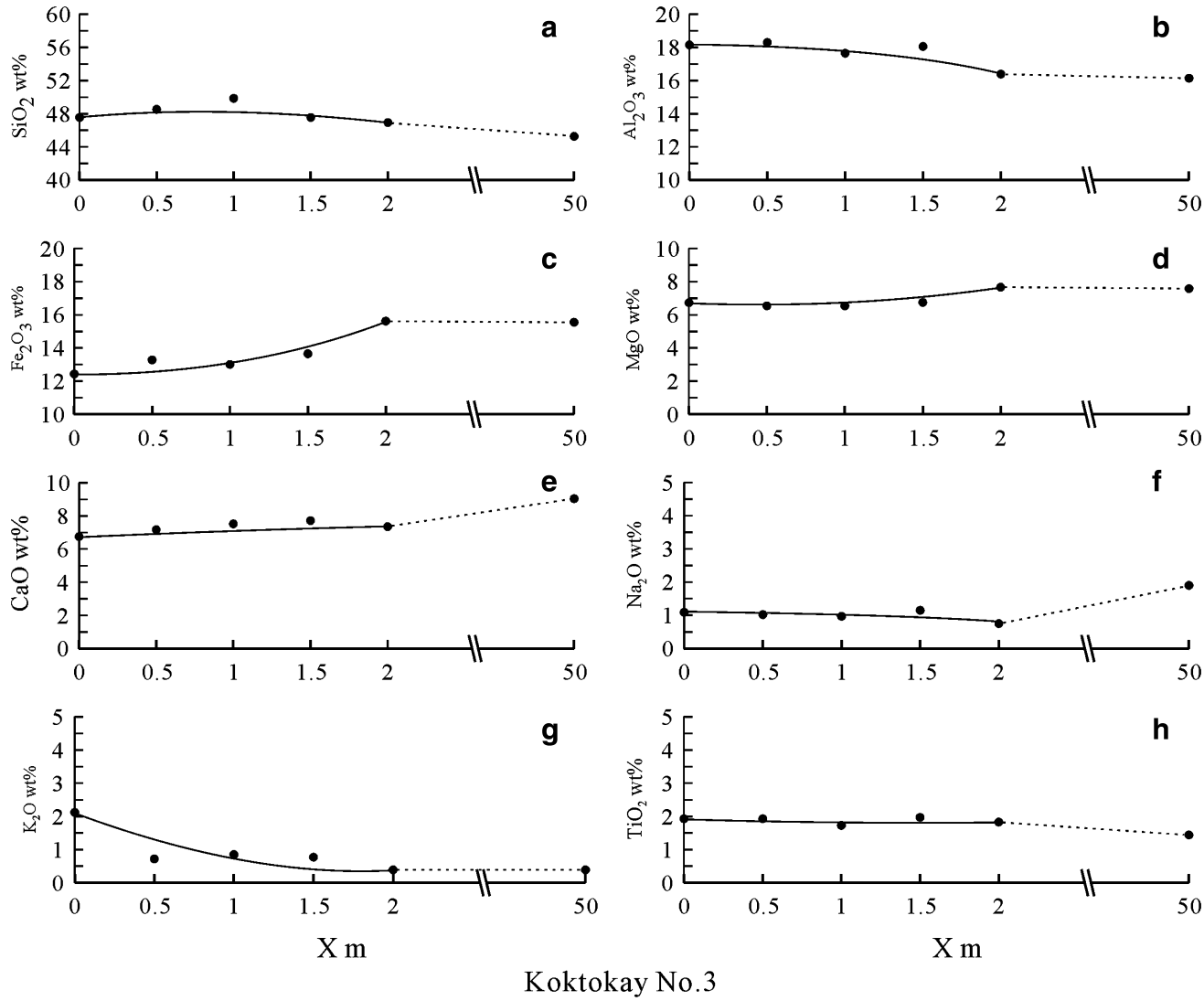

Fig. 4 The content variations of major elements (SiO_2, Al_2O_3, Fe_2O_3, MgO, CaO, Na_2O, K_2O, and TiO_2) in wall rock alteration belt with distance from pegmatite contact of the Koktokay No. 3

biotite, tourmaline, muscovite, and chlorite during hydrothermal alteration. Undoubtedly, hornblende of the unaltered amphibolite may have provided Fe and Mg for the formation of biotite, tourmaline, and chlorite; whereas K and Al in biotite and B, Li, and Al in tourmaline could have been provided by the exsolved magmatic fluid of the pegmatite-forming melt. The associated alteration reactions can be expressed simply as follows:

$$\begin{aligned}&2Ca_2Na(Mg,Fe)_4Fe[Si_4O_{11}]_2(OH)_2(Hbl)+2Al^{3+}\\&+2K^+ + O^{2-} = 2K\left\{(Mg,Fe)_3[Si_3AlO_{10}](OH)_2\right\}(Bio)\\&+4Ca^{2+}+2Na^{+}+2Fe^{2+}+2Fe^{3+}+5Si_2O_5^{2-}\end{aligned} \quad (1)$$

$$\begin{aligned}&2Ca_2Na(Mg,Fe)_4Fe[Si_4O_{11}]_2(OH)_2(Hbl)+12Al^{3+}+6H_3BO_3\\&+15O^{2-}=2Na(Mg,Fe)_3Al_6[Si_6O_{18}](BO_3)_3(OH)_4(Tour)\\&+4Ca^{2+}+2Mg^{2+}+2Fe^{2+}+4SiO_3^{2-}+2Fe^{3+}+7H_2O\end{aligned} \quad (2)$$

$$\begin{aligned}&Ca_2Na(Mg,Fe)_4Fe[Si_4O_{11}]_2(OH)_2(Hbl)+3Fe^{3+}+3H_2O+9O^{2-}\\&=(Mg,Fe)_4Fe_4Si_2O_{10}(OH)_8(Chl)+2Ca^{2+}+Na^{+}+6SiO_3^{2-}\end{aligned} \quad (3)$$

$$\begin{aligned}&3Na[AlSi_3O_8]\,(Pl)+H_2O+K^+\\&=K\left\{Al_2[Si_3AlO_{10}](OH)_2\right\}(Mus)+3Na^{+}+6SiO_3^{2-}\end{aligned} \quad (4)$$

5.2 Migrations of component/element based on mass-balance calculation

Not only were there component gains and losses in the metasomatic alteration zone, there was also a volume change during interaction of the host rock with the exsolved magmatic fluid. The isocon plot proposed by Grant (1986) has been applied extensively to estimate migrations of

Table 3 Trace element and REE concentrations (in ppm) in altered and unaltered host rocks surrounding the Koktokay No. 3 pegmatite

	Kp03-alt-01	Kp03-alt-02	Kp03-alt-03	Kp03-alt-04	Kp03-alt-05	Kp03-hr-02
Li	693	589.5	523	476	442	153.67
Be	2.87	1.29	0.96	1.41	0.88	1.11
Rb	160	71.49	60.5	53	22.2	20.80
Cs	81.8	46.71	43.3	33	15.3	8.26
Nb	11.2	9.46	8.78	10.7	7.47	3.48
Ta	0.68	0.56	0.56	0.62	0.48	0.25
Y	15.8	8.07	11.7	16	12	16.30
La	14.00	8.12	15.30	15.00	6.03	7.37
Ce	30.00	14.86	30.40	32.70	12.80	18.50
Pr	3.68	1.99	3.46	3.87	1.68	2.50
Nd	16.40	8.69	14.40	18.20	7.69	11.20
Sm	3.85	1.86	3.14	4.31	1.98	2.65
Eu	1.21	1.11	1.18	1.27	0.97	0.82
Gd	3.75	1.82	3.30	4.60	2.20	2.74
Tb	0.58	0.26	0.45	0.66	0.38	0.48
Dy	3.18	1.49	2.38	3.48	2.28	2.92
Ho	0.62	0.32	0.46	0.66	0.48	0.62
Er	1.71	0.86	1.26	1.76	1.47	1.77
Tm	0.25	0.13	0.17	0.23	0.22	0.26
Yb	1.50	0.88	1.07	1.37	1.42	1.70
Lu	0.25	0.15	0.17	0.23	0.21	0.25
$\sum$REE	96.78	50.62	88.82	104.33	51.82	70.08
δEu	0.98	1.84	1.12	0.87	1.42	0.93
$(La/Sm)_N$	2.29	2.74	3.07	2.19	1.92	1.75
$(La/Gd)_N$	3.12	3.73	3.88	2.72	2.29	2.25
$(La/Yb)_N$	6.29	6.20	9.64	7.38	2.86	2.92

components and elements during metasomatism alteration processes (Guo et al. 2009, 2013; Chen et al. 2016). Based on mass-balance, the concentration equation for a given mobile component (m) can be re-written as:

$$\Delta C_m^{O-A} = \left(C_i^O / C_i^A\right) C_m^A - C_m^O \quad (5)$$

In which, C_i^O and C_i^A denote the concentration of the immobile component (i) in the original unaltered (O) and altered (A) host rock, C_m^O and C_m^A denote the concentration of mobile component (m) in the original unaltered and altered host rock, and ΔC_m^{O-A} represents the concentration difference of the mobile component between the original unaltered and altered host rock.

Usually, REEs are thought to be inactive in alteration processes. Assumed to be the most immobile REE (Kessel et al. 2005), Yb was chosen to estimate the component/element migration ratios ($\delta = \Delta C_m^{O-A}/C_m^O$) in this study. The contact zone is not only the lithological interface, but also a water–rock interaction interface, representing the most intensive substance exchange between pegmatite and host rock during hydrothermal alteration. According to the concentrations of components and elements in the contact zone (Kp03-alt-01) and the unaltered host rock (Kp03-hr-02), the calculated component/element migration ratios are listed in Table 4, and the isocon plot in Fig. 7. For the main chemical compositions, the order of positive migration ratios was $P_2O_5 > K_2O > TiO_2 > Al_2O_3 > SiO_2 > MnO \geq MgO$, meaning that these components migrated in, whereas migration ratios for CaO, Na_2O, and Fe_2O_3 were negative, indicating that these components migrated out with an order of $Na_2O > CaO > Fe_2O_3$. For rare elements, the migration ratios were positive values with an order of Cs > Rb > Li > Nb > Ta > Be, signifying that all rare elements migrated from the exsolved magmatic fluid into the altered host rocks.

It has been reported that Li, Rb, and Cs are highly mobile and form large dispersion halos (Selway and Breaks 2005; Galeschuk and Vanstone 2007; Shearer et al. 1986), with Li thought to have the greatest mobility among these elements (Beus et al. 1968; Trueman 1978; Shearer et al. 1986). However, there is no agreement on the relative mobility of Rb and Cs. Beus et al. (1968) suggested a relative mobility of Li > Cs > Rb, whereas Trueman (1978) and Shearer et al. (1986) fixed the relative mobilities with the order of Li > Rb > Cs. Although migration

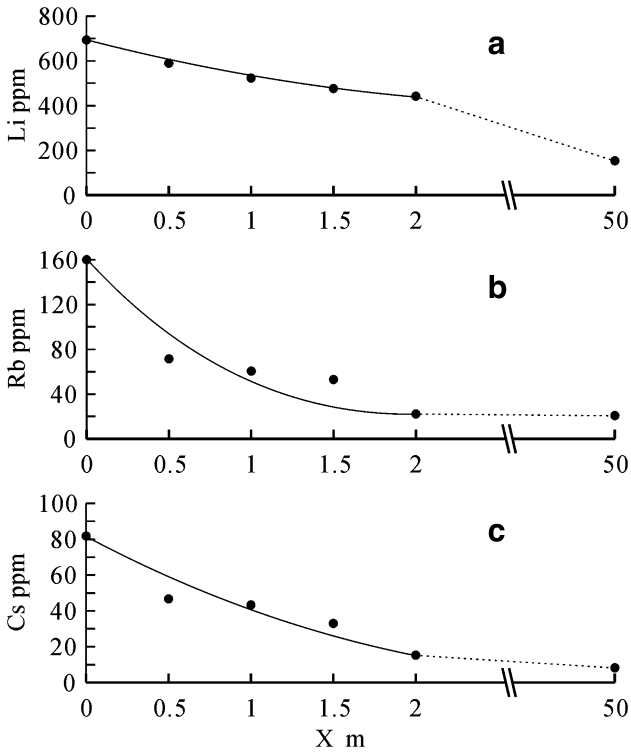

Fig. 5 The content variations of Li, Be, and Rb in wall rock alteration belt with distance from pegmatite contact of the Koktokay No. 3

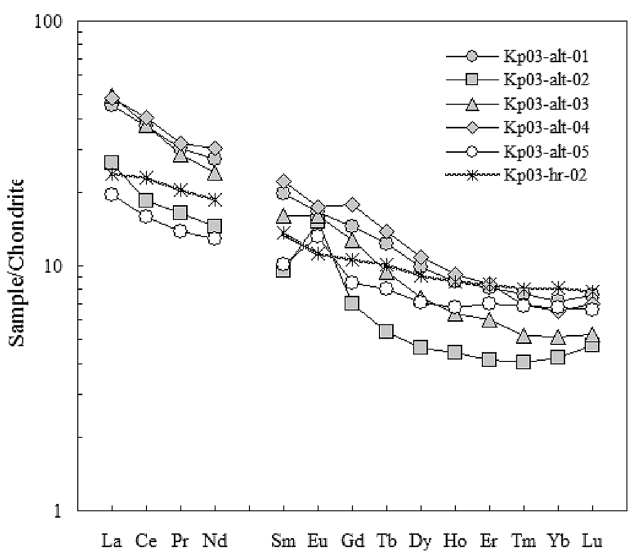

Fig. 6 The chondrite-normalized REE patterns of the altered and unaltered host rocks

ratios show an order of Cs > Rb > Li in this study, we propose a mobility of Li > Cs > Rb based on relatively higher Li contents and on Cs being distributed in the weakly altered host rocks (Kp03-alt-05) surrounding the Koktokay No. 3 pegmatite.

The Koktokay No. 3 pegmatite hosts a super-large rare metal ore deposit in the Chinese Altay orogenic belt. The results of this study indicate that Li, Rb, and Cs contents in the altered host rock and their migration ratios can be used as an indicator to evaluate mineralization potential of pegmatite in the Chinese Altay. If a contact zone, which originated from intrusion of pegmatite into amphibolite, has similar Li, Rb, and Cs contents as those in the studied contact zone around the Koktokay No. 3 pegmatite (at least 700 ppm Li, 160 ppm Rb, and 80 ppm Cs) and the migration ratios of Li, Rb, and Cs are more than 4, 7, and 10, respectively, rare metal mineralization in the interior of the pegmatite is probably indicated.

5.3 Migration of rare elements during hydrothermal alteration

Migration of rare elements in fluid includes diffusion and infiltration processes. For porosity (ε) of host rock ≪ 1, the main control of element migration in fluid through host rock is diffusion; infiltration is negligible. Therefore, according to the study on ore-forming element migration in the altered country rock of No. 807 pegmatite vein in Kalu'an, we set up a diffusion model under conditions of very low porosity of biotite-quartz schist (ε = 0.093, Chen et al. 2016). Because the porosity of the amphibolite surrounding the Koktokay No. 3 pegmatite is very low (ε = 0.0183, Trčlková 2005), only diffusion in the altered host rock was taken into consideration in this study. The diffusion equation of ore-forming elements can be simplified as:

$$C_{(x,t)}/C_o = erfc\left(\frac{x}{2\sqrt{D_{eff}t}}\right) \quad (6)$$

In which, C_0 and $C_{(x,t)}$ denote the initial concentration and actual concentration of rare elements in fluid and in host rock at a distance of x (x = 0.0–2.0 m), x and t are diffusion distance and time, and D_{eff} represents the effective diffusion coefficient.

According to Chen et al. (2016), D_{eff} can be expressed as:

$$D_{eff} = \frac{\varepsilon}{\tau}\frac{RT\lambda_m^{\infty}}{Z^2F^2}\exp\left(-\frac{E}{RT}\right) \quad (7)$$

The definitions and connotations of associated parameters in the above expression can be found in Chen et al. (2016) and references therein.

Although the concentrations of F and Cl in the altered minerals (hornblende, biotite, tourmaline, and chlorite) and

Table 4 Quantitative mass-balance calculation results of altered wallrock at pegmatite contact ($\delta = \Delta C_m^{O-A}/C_m^O$)

Major element	SiO_2	TiO_2	Al_2O_3	Fe_2O_3	MnO_2	MgO	CaO	Na_2O	K_2O	P_2O_5
δ	0.19	0.52	0.27	−0.11	0.03	0.01	−0.15	−0.35	5.49	6.22
Rare element	Li	Be	Rb	Nb	Cs	Ta	Yb			
δ	4.11	1.92	7.72	2.65	10.22	2.11	0			

Yb is assumed to be the most immobile component; the background sample is treated as the original unaltered rock. Positive value indicates gain; negative value, loss

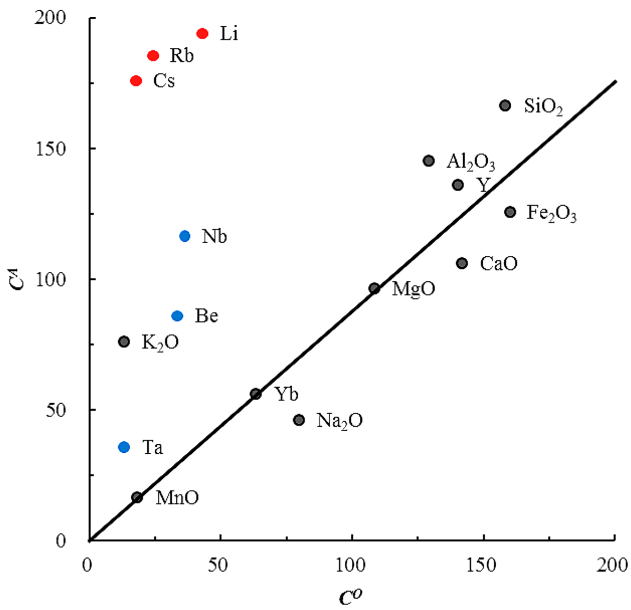

Fig. 7 Isocon diagram showing the mass transfer from the host rock of the Koktokay No. 3

in the altered and unaltered host rocks surrounding the Koktokay No. 3 pegmatite were not determined in this study, previous studies showed that only F incorporated into the tourmalines from the exocontact zone with a maximum value 1.33 wt% F (Zhang 2001, 2005; Wu et al. 2015). In addition, the exsolved magmatic fluid from the late magmatic melt was deduced to be concentrated in K–Li–Rb–Cs–Ta–Al–F(Cl)–B based on a comparison of chemical composition of the strongly altered host rock with that of the unaltered host rock (Zhang 2001). As the reported salinity of fluid inclusions from textural zones IV–VI was in the range of 10 wt%–18 wt% NaCl eqv (Zhu et al. 2000), it was deduced that in addition to F, Cl is also an important complexing agent in the exsolved magmatic fluid, dominating the migration of rare elements during hydrothermal alteration of the host rock. As an unknown parameter, the effective diffusion coefficient (D_{eff}) comes from calculation based on the molar conductivity (λ_m^∞). Since F and Cl in the fluid have a great effect on the migration of rare elements (Linnen et al. 2012), and thus far there is no available molar conductivity (λ_m^∞) of LiCl, RbCl, and CsCl, we have chosen F as the main complexing agent for establishment of the rare elements diffusion model. Therefore, the effective diffusion coefficients (D_{eff}) of LiF, RbF, and CsF were estimated under fluid temperature of 500–550 °C (Table 5).

Based on expression (6), it can be seen that concentration changes of ore-forming elements ($C_{(x,t)}$) as through diffusion are dependent on initial concentration of elements in fluid (C_0), effective diffusion coefficient (D_{eff}), diffusion distance (x), and diffusion time (t). Since there is an existing negative correlation between x and $C_{(x,t)}$, it is clear that diffusion is transporting more, farther if the concentration of ore-forming elements decreases slowly with increasing distance.

From the above, the function relation between $C_{(x,t)}$ and x was fitted after ore-forming element contents in the altered and unaltered host rocks were substituted into the diffusion Eq. (6) (Fig. 8). Obviously, concentration variation with distance of LiF, RbF, and CsF in the altered host rocks meet the basic requirement of diffusion. The order of migration distance is LiF > CsF > RbF, corresponding to diffusion times of $(3.39 \pm 0.35) \times 10^6$, $(3.19 \pm 0.28) \times 10^5$, and $(6.33 \pm 0.05) \times 10^5$ years, respectively.

Table 5 Calculated effective diffusion coefficients and diffusion times of LiF, RbF and CsF in altered amphibolite surrounding the Koktokay No. 3 pegmatite

Parameter	LiF	RbF	CsF	References
λ_m^∞ (S cm^2 mol^{-1})	94.1	133.2	132.6	Lou (1999)
E (J mol^{-1})	20,600	24,100	22,200	Ejima et al. (1987)
ε		0.0183		Trčlková (2005)
T (K)		773–823		Zhu et al. (2000)
$D_{eff} \times 10^{-10}$ (cm^2/s)	3.76 ± 0.36	3.15 ± 0.36	4.17 ± 0.44	This study
$t \times 10^5$ (a)	4.91 ± 0.48	5.58 ± 0.63	6.93 ± 0.72	

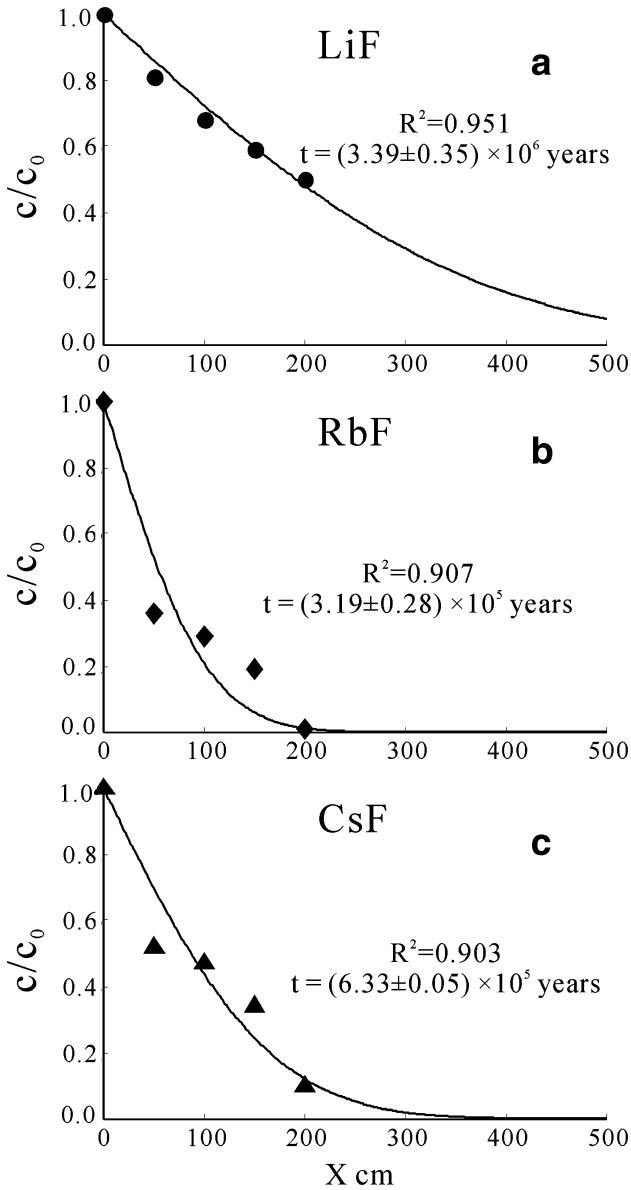

Fig. 8 The idealized model diagram for diffusion–infiltration of LiF, RbF, CsF

6 Conclusions

1. The alteration zone surrounding the Koktokay No. 3 pegmatite is in the range of 2.0 m, and characterized by biotitization, tourmalization, and chloritization. During hydrothermal alteration, hornblende provides Fe and Mg for the formation of biotite, tourmaline, and chlorite; whereas K and Al in biotite and B, Li, and Al in tourmaline were probably provided by the exsolved magmatic fluid.
2. Li, Rb, and Cs contents in the altered host rocks were much higher than those in the unaltered host rocks were, and show a decreasing trend with distance from the contact. The chondrite-normalized REE of the altered and unaltered host rock shows a right-inclined pattern from La to Lu, but enrichment of light over heavy REEs after hydrothermal alteration.
3. The migration ratios are positive values with an order of Cs > Rb > Li > Nb > Ta > Be, signifying that all rare elements migrated from the exsolved magmatic fluid into the altered host rocks.
4. Diffusion is the only mechanism for migration of ore-forming elements in the alteration zone. The order of migration distance is LiF > CsF > RbF, corresponding to diffusion times of $(3.39 \pm 0.35) \times 10^6$, $(3.19 \pm 0.28) \times 10^5$, and $(6.33 \pm 0.05) \times 10^5$ years, respectively.

Acknowledgements We thank engineer Maode Shen and engineer Fang Xia for their help in the sample collection. We are grateful to engineer Xianglin Tu for experimental assistance. This study was supported jointly by the Natural Science Foundation of China (Grant No. 41372104) and Research Project of Xinjiang Nonferrous Metals Industry (Group) Co., Ltd. (Grant No. YSKY2011-02).

References

Beus AA, Berengilova VV, Grabovskaya LI, Kochemasov LA, Leonteva LA, Sitnin AA (1968) Geochemical prospecting for endogenous ore deposits of rare elements (e.g. for tantalum): Academy of Science USSR, Dept. of Geology of USSR, Institute of Mineralogy, Geochemistry and Crystal Chemistry of Rare Elements, Moscow, USSR (Translated by the Department of the Secretary of State, Ottawa, Canada)

Breaks FW, Tindle AG (1997) Rare element exploration potential of the Separation Lake area: An emerging target for Bikita-type mineralization in the Superior province of northwest Ontario. In: Summary of field work and other activities 1997. Ontario Geological Survey, Miscellaneous Paper 168, pp 72–88

Breaks FW, Selway JB, Tindle AG (2003) Fertile peraluminous granites and related rare-element mineralization in pegmatites, Superior Province, northwest and northeast Ontario: Operation Treasure Hunt; Ontario Geological Survey. Open File Rep 6099:179

Cai K, Sun M, Yuan C, Long X, Xiao W (2011a) Geological framework and Paleozoic tectonic history of the Chinese Altai, NW China: a review. Russ Geol Geophys 52:1619–1633

Cai K, Sun M, Yuan C, Zhao G, Xiao W, Long X, Wu F (2011b) Geochronology, petrogenesis and tectonic significance of peraluminous granites from the Chinese Altai, NW China. Lithos 127:261–281

Černý P (1989) Exploration strategy and methods for pegmatite deposits of tantalum. In: Moller P, Cerny P, Saupe F (eds) Lanthanides, tantalum, and niobium. Springer, New York, pp 274–302

Che XD, Wu FY, Wang RC, Gerdes Axel, Ji WQ, Zhao ZH, Yang JH, Zhu ZY (2015) In situ U–Pb isotopic dating of columbite–tantalite by LA–ICP–MS. Ore Geol Rev 65:979–989

Chen J (2011) Geochemistry of the part of the plate of the Altai No. 3 Pegmatite and its Formation and Evolution. Dissertation, Institute of Geochemistry, Chinese Academy of Sciences **(in Chinese with English abstract)**

Chen Y, Zhang H, Zhao JY (2016) Altered country rock of No. 807 pegmatite vein in Kalu'an ore area, Xinjiang: ore-forming

element diffusion model and its influencing factors. Geochimica 45(3):268–280

Ejima T, Sato Y, Yaegashi S, Kijima T, Takeuchi E, Tamai K (1987) Visosity of molten alkali fluorides. J Jpn Inst Met 51(4):328–337

Galeschuk C, Vanstone P (2007) Exploration techniques for rare-element pegmatite in the Bird River greenstone belt, Southeastern Manitoba. In: Milkereit B (ed) Proceedings of exploration 07: fifth decennial international conference on mineral exploration, pp 823–839

Grant JA (1986) The isocon diagram: a simple solution to gresens equation for metasomatic alteration. Econ Geol 81(8):1976–1982

Guo S, Ye K, Chen Y, Liu JB (2009) A normalization solution to mass transfer illustration of multiple progressively altered samples using the Isocon diagram. Econ Geol 104:881–886

Guo S, Ye K, Chen Y, Liu JB, Zhang LM (2013) Introduction of mass-balance calculation method for component transfer during the opening of a geological system. Acta Petrol Sin 29(5):1486–1498

Kessel R, Schmidt MW, Ulmer P, Pettke T (2005) Trace element signature of subduction-zone fluids, melts and supercritical liquids at 120–180 km depth. Nature 437(7059):724–727

Liang Q, Jing H, Gregoire DC (2000) Determination of trace elements in granites by inductively coupled plasma mass spectrometry. Talanta 51(3):507–513

Linnen RL, Van Lichtervelde M, Cerny P (2012) Granitic pegmatites as sources of strategic metals. Elements 8(4):275–280

Liu CQ, Zhang H (2005) The lanthanide tetrad effect in apatite from the Altay No. 3 pegmatite, Xingjiang, China: an intrinsic feature of the pegmatite magma. Chem Geol 214:61–77

Liu F, Zhang ZX, Li Q, Zhang Q, Li C (2014) New precise timing constraint for the Keketuohai No. 3 pegmatite in Xinjiang, China, and identification of its parental pluton. Ore Geol Rev 56(1):209–219

London D (1986) Holmquistite as a guide to pegmatitic rare metal deposits. Econ Geol 81:704–712

London D, Morgan GB 6th, Wolf MB (1996) Boron in granitic rocks and their contact aureoles. Rev Mineral Geochem 33:299–330

Long XP, Sun M, Yuan C, Xiao W, Lin S, Wu F, Xia X, Cai K (2007) U–Pb and Hf isotopic study of zircons from metasedimentary rocks in the Chinese Altai: implications for Early Paleozoic tectonic evolution. Tectonics 26:TC5015

Long XP, Sun M, Yuan C, Xiao WJ, Cai KD (2008) Early Paleozoic sedimentary record of the Chinese Altai: implications for its tectonic evolution. Sed Geol 208(3–4):88–100

Long XP, Yuan C, Sun M, Xiao WJ, Zhao GC, Wang YJ, Cai KD (2010) Detrital zircon ages and Hf isotopes of the Early Paleozoic Flysch sequence in the Chinese Altai, NW China: new constraints on depositional age, provenance and tectonic evolution. Tectonophysics 180:213–231

Lou C (1999) Conductance measurements part 1 theory. Bioanalytical Systems Inc, pp 91–96

Lu H, Wang Z, Li Y (1996) Magma–fluid transition and genesis of pegmatite dike No. 3 at Altay, Xinjiang. Acta Mineral Sin 16(1):1–7 **(in Chinese with English abstract)**

Selway JB, Breaks FW (2005) A review of rare-element (Li–Cs–Ta) pegmatite exploration techniques for the Superior Province, Canada, and large world tantalum deposits. Explor Min Geol 14:1–30

Sengör AMC, Natalín BA, Burtman VS (1993) Evolution of the Altaid tentonic collage and Paleozoic crustal growth in Eurasia. Nature 364:299–307

Shearer CK, Papike JJ, Simon SB (1986) Pegmatite–wallrock interactions, Black Hills, South Dakota: Interaction between pegmatite-derived fluids and quarts-mica schist wallrock. Am Mineral 71:518–539

Sun M, Yuan C, Xiao W, Long X, Xia X, Zhao G, Lin S, Wu F, Kröner A (2008) Zircon U–Pb and Hf isotopic study of gneissic rocks from the Chinese Altai: progressive accretionary history in the Early to Middle Palaeozoic. Chem Geol 247:352–383

Sun M, Long XP, Cai KD, Jiang YD, Wong PW, Yuan C, Zhao GC, Xiao WJ, Wu FY (2009) Early Paleozoic ridge subduction in the Chinese Altai: insight from the abrupt change in zircon Hf isotopic compositions. Sci China Ser D 39:1–14

Trčlková J (2005) Physical, mechanical and deformational properties of metabasalts, amphibolites and gneisses from KSDB-3 compared with surface analogues. Acta Geodyn Geomater 4(140):39–47

Trueman DL (1978) Exploration methods in the Tanco mine area of southeastern Manitoba, Canada. Energy 3:293–297

Wang DH, Chen YC, Li HY, Xu ZG, Li TD (1998) Mantle degassing of the Altai orogenic belt: insight from helium isotope study. Chin Sci Bull 43(23):2541–2544 **(in Chinese)**

Wang T, Hong DW, Jahn BM, Tong Y (2006) Timing, petrogenesis, and setting of Paleozoic synorogenic intrusions from the Altai Mountains, Northwest China: implications for the tectonic evolution of an accretionary orogen. J Geol 114:735–751

Wang T, Tong Y, Jahn BM et al (2007) SHRIMP U–Pb zircon geochronology of the Altai No. 3 pegmatite, NW China, and its implications for the origin and tectonic setting of the pegmatite. Ore Geol Rev 32:325–336

Wang RC, Che XD, Zhang WL, Zhang AC, Zhang H (2009) Geochemical evolution and late re-equilibration of Na-Cs-rich beryl from the Koktokay #3 pegmatite (Altai, NW China). Eur J Mineral 21:795–809

Windley BF, Kröner A, Guo J, Qu G, Li Y, Zhang C (2002) Neoproterozoic to Paleozoic geology of the Altai orogen, NW China: new zircon age data and tectonic evolution. J Geol 110:719–737

Windley BF, Alexeiev D, Xiao WJ, Kröner A, Badarch G (2007) Tectonic models for accretion of the Central Asian Orogenic Belt. J Geol Soc 164:31–47

Wu SR, Zhao JY, Zhang X, Zhang H (2015) Magmatic-hydrothermal evolution of the Koktokay No. 3 Pegmatite, Altay, NW China: evidence from compositional variation of tourmaline. Acta Mineral Sin 35(3):299–308 **(in Chinese with English abstract)**

Xiao WJ, Windley BF, Badarch G, Sun S, Li JL, Qin KZ, Wang Z (2004) Palaeozoic accretionary and convergent tectonics of the southern Altaids: implications for the growth of central Asia. J Geol Soc Lond 161:339–342

Yuan C, Sun M, Xiao WJ, Li XH, Chen HL, Lin SF, Xia XP, Long XP (2007) Accretionary orogenesis of the Chinese Altai: insights from Paleozoic granitoids. Chem Geol 242(1):22–39

Zhang H (2001) The geochemical behaviors and mechanisms of incompatible trace elements in the magmatic-hydrothermal transition system: A case study of Altai No. 3 pegmatite, Xinjiang. Dissertation, Institute of Geochemistry, Chinese Academy of Sciences **(in Chinese with English abstract)**

Zhang AC (2005) Mineralogy of the Koktokay No.3 pegmatite, Xinjiang: record of magmatic-hydrothermal evolution, Department of Earth Sciences, Nanjing University, pp 56–63 **(in Chinese with English abstract)**

Zhang AC, Wang RC, Hu H, Chen XM (2004) Occurrences of foitite and rossmanite from the Koktokay No. 3 granitic pegmatite dyke, Altai, northwestern China: a record of hydrothermal fluids. Can Mineral 42:873–882

Zhu JC, Wu CN, Liu CS, Li FC, Huang XL, Zhou DS (2000) Magmatic-hydrothermal evolution and genesis of Koktokay No. 3 rare metal pegmatite dyke, Altai, China. Geol J China Univ 6:40–52 **(in Chinese with English abstract)**

Zhu YF, Zeng YS, Gu LB (2006) Geochemistry of the rare metal-bearing pegmatite No. 3 vein and related granites in the Keketuohai region, Altay Mountains, northwest China. J Asian Earth Sci 27(1):61–77

Zou TR, Li QC (2006) Rare and rare earth metallic deposits in Xinjiang, China. Geological Publishing House, Beijing 1–284 **(in Chinese with English abstract)**

Zou TR, Zhang XC, Jia FY, Wang RC, Cao HZ, Wu PQ (1986) A discussion about contributing factor of the Altai No. 3 pegmatite. Mineral Depos 5:34–48 **(in Chinese with English abstract)**

Zou TR, Cao HZ, Wu BQ (1989) Orogenic and anorogenic granitoids of Altay Mountains of Xinjiang and their discrimination criteria. Acta Geol Sin 2:45–64